Fluid Phase Equilibria 335 (2012) 46–59

Contents lists available at SciVerse ScienceDirect

Fluid Phase Equilibria

journal homepage: www.elsevier.com/locate/fluid

Critical parameters optimized for accurate phase behavior modeling for heavy n-alkanes up to C_{100} using the Peng–Robinson equation of state

Ashutosh Kumar, Ryosuke Okuno*

University of Alberta, Edmonton, Alberta, Canada T6G 2W2

ARTICLE INFO

Article history:
Received 22 April 2012
Received in revised form 21 July 2012
Accepted 31 July 2012
Available online 28 August 2012

Keywords:
Equations of state
Critical parameters
Petroleum fluids
Fluid characterization
Heavy oils

ABSTRACT

The Peng–Robinson equation of state (PR EOS) is widely used for modeling phase behavior of hydrocarbon mixtures. When applied to heavy hydrocarbons and their mixtures, however, the PR EOS can exhibit erroneous phase behavior predictions. In this research, we develop new correlations for critical temperatures (T_C), critical pressures (P_C), and acentric factors (ω) that enable the PR EOS to accurately predict phase behavior of n-alkanes up to C_{100}.

Predictions using the PR EOS with the new correlations give 3.0% average absolute deviation (AAD) for 3583 density data, and 3.4% AAD for 1525 vapor pressure data for n-alkanes from C_7 to C_{100}. Significant improvement is also observed for bubble point pressure and density predictions for n-alkane mixtures. The new correlations developed for T_C, P_C, and ω are then applied for characterizing 25 different reservoir oils. Results show that, compared to the conventional critical parameter correlations in the literature, our correlations give more accurate phase behavior predictions while requiring less adjustment of the parameters. The optimum T_C and P_C developed for n-alkanes can serve as useful lower limits for T_C and P_C of pseudo components of reservoir oils that are characterized using the PR EOS.

1. Introduction

Cubic equations of state (EOSs) are widely used in the petroleum industry to model volumetric and compositional phase behavior of petroleum reservoir fluids. Since the original research of van der Waals [1] in 1873, many cubic EOSs have been developed including the Peng–Robinson (PR) EOS [2,3] and the Soave–Redlich–Kwong (SRK) EOS [4]. These cubic EOSs are used in compositional reservoir simulation to design enhanced oil recovery (EOR) using solvents. With recent advances in the EOS compositional reservoir simulation technology, it is now possible to robustly simulate complex gas/CO_2 injection processes that involve critical endpoint behavior [5].

Reliable predictions of EOR using compositional reservoir simulation require accurate characterization of reservoir fluids using a cubic EOS. Such characterization methods have been developed, and implemented in commercial software for conventional oils [6–11]. Characterization of heavy oils using an EOS, however, is more difficult than that of conventional oils. Firstly, compositions of heavy oils are highly uncertain in terms of the concentration of each carbon number (CN) group and the paraffins–naphthenes–aromatics (PNA) distribution within each CN group. Secondly, critical parameters required in EOS fluid characterization are unknown for hydrocarbons heavier than tetracosane, C_{24} [12]. Thirdly, accurate prediction of heavy oil densities is difficult using two-parameter cubic EOSs with a constant critical compressibility factor such as the PR and SRK EOSs [2–4]. A cubic EOS with more than two parameters can improve density predictions for heavy oils [13], but at the expense of computational efficiency.

In the literature, a few different sets of correlations were proposed for critical temperature (T_C), critical pressure (P_C), and acentric factor (ω) extrapolated for hydrocarbons heavier than C_{24} [14,15]. These correlations, however, were developed based on reservoir oil samples, and do not explicitly account for effects of the PNA distribution on critical parameters. Since a heavier CN group can contain a wider variety of compounds, more uncertainties in phase behavior predictions arise when such generic correlations are used for heavy oil characterization.

Cubic EOSs are incapable of accurate prediction of densities and vapor pressures for heavy hydrocarbons even when accurate critical parameters are known and used. The volume shift approach of Péneloux et al. [16] (Jhaveri and Youngren [17] for the PR EOS) is widely used to improve density predictions with cubic EOSs. The volume shift approach, however, does not improve compositional phase behavior predictions. Use of volume shift in EOS fluid characterization can cause erroneous oil recovery predictions in

* Corresponding author at: University of Alberta, Department of Civil & Environmental Engineering, School of Petroleum Engineering, 3-114 Markin/CNRL Natural Resources Engineering Facility, Edmonton, Alberta, Canada T6G 2W2.
Tel.: +1 780 492 6121; fax: +1 780 492 0249.
E-mail address: rokuno@ualberta.ca (R. Okuno).

0378-3812/$ – see front matter © 2012 Elsevier B.V. All rights reserved.
http://dx.doi.org/10.1016/j.fluid.2012.07.029

simulation of miscible gas injection, where mass transfer among phases is significant [18].

Another approach for improving the PR EOS is to modify the alpha function [19–24]. These modified alpha functions can improve vapor pressure predictions for heavy hydrocarbons. However, they change the functional form of the PR EOS, which does not allow for direct application with commercial reservoir simulators.

Ting et al. [25] and Voutsas et al. [26] fitted the critical parameters for the PR EOS to density and vapor pressure data for selected hydrocarbons and their binary mixtures. They considered n-alkanes $C_1, C_2, C_3, C_4, C_6, C_7, C_{10}, C_{16}, C_{18}, C_{20}, C_{24}, C_{30}, C_{36}$, and C_{40} for their critical parameter optimization. They presented that the PR EOS with the fitted critical parameters exhibits accurate phase behavior predictions for the fluids studied. This approach keeps the functional form of the PR EOS, and minimizes use of volume shift. However, no attempt has been made to optimize the critical parameters for the PR EOS for a wide CN range that is common for reservoir oils.

In this research, we develop optimized values and new correlations for T_C, P_C, and ω for accurate phase behavior predictions for heavy n-alkanes up to C_{100} using the PR EOS. Our development is focused on a homologous series of n-alkanes mainly because more data are available for n-alkanes than for the other types of hydrocarbons. For characterization of actual oils, the effects of N and A components on phase behavior predictions can be considered by perturbations from n-alkanes' critical parameters as proposed by Quiñones-Cisneros et al. [27].

The subsequent sections present our development of optimized T_C, P_C, and ω along with experimental data used. We then develop new correlations based on the optimized values for T_C, P_C, and ω. The new set of critical parameters is used to demonstrate improved predictions of densities and vapor pressures of n-alkanes and their mixtures. We also present application of the optimum critical parameters for characterizing 25 different reservoir oils.

2. Optimization of critical parameters

The PR EOS is one of the most widely used cubic EOSs in the petroleum industry. It uses two parameters as given below.

$$P = \frac{RT}{v-b} - \frac{a_C\alpha(T)}{V^2+2bv-b^2}, \tag{1}$$

where

$$a_C = 0.457235529\frac{(RT_C)^2}{P_C} \tag{2}$$

$$\sqrt{\alpha(T)} = \left[1 + m\left(1 - \left(\frac{T}{T_C}\right)^{0.5}\right)\right] \tag{3}$$

$$m = 0.37464 + 1.54226\omega - 0.26992\omega^2 \quad \text{for } \omega < 0.49 \tag{4}$$

$$m = 0.379642 + 1.48503\omega - 0.164423\omega^2 + 0.016666\omega^3 \quad \text{for } \omega \geq 0.49 \tag{5}$$

Eqs. (4) and (5) indicate that the $m(\omega)$ function is one-to-one as shown in Fig. 1; i.e., a given positive real value for ω results in a unique value for m, and vice versa. Our optimization is performed in terms of T_C, P_C, and m. It is easy to derive ω corresponding to an optimized m.

2.1. Experimental data used for optimization

Our optimization uses experimental data for vapor pressure and liquid density of n-alkanes. Table A1 summarizes the sources and T–P ranges of data used for the optimization. Table 1 lists the n-alkanes for which experimental data are available for liquid densities and vapor pressures, and data uncertainties for each of the compounds.

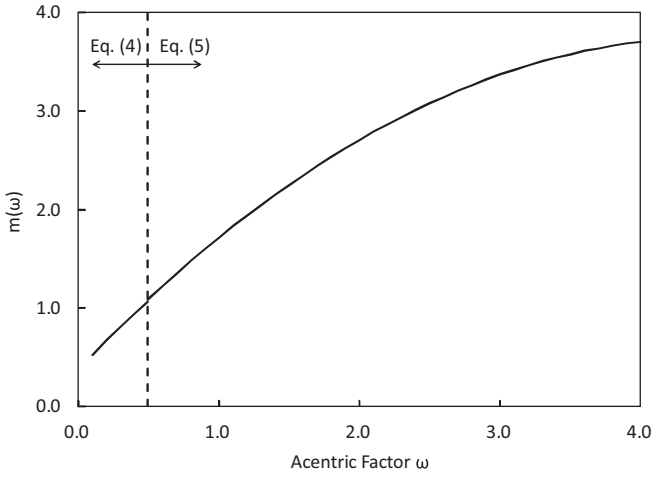

Fig. 1. The $m(\omega)$ function for the Peng–Robinson EOS as defined in Eqs. (4) and (5).

Saturated liquid densities estimated in Yaws [28] are used for n-alkanes that have no liquid density data available in the literature (Table A1 shows for which n-alkanes the estimations of Yaws [28] are used). The estimation of saturated liquid densities is based on a modified form of the Rackett equation [29] using four parameters [30]. The quality of the estimations in Yaws [28] is difficult to judge owing to the lack of experimental data. However, the modified Rackett equation represents experimental data very well [31]. Poling et al. [31] recommended the modified Rackett equation for estimation of saturated liquid densities.

Vapor pressure data for many n-alkanes are not available in the literature. Therefore, vapor pressure data for such n-alkanes are supplemented by the correlation of Riazi and AlQaheem [32] given by Eq. (6).

$$\ln P_r^{\text{vap}} = (a_1 + a_2 r + a_3 r^2) + (b_1 + b_2 r + b_3 r^2)T_r^{-2} + (c_1 + c_2 r)T_r \tag{6}$$

Table 1
Uncertainties in experimental data that are used in our optimization in Section 2.

n-Alkanes	Density data uncertainty	Vapor pressure data uncertainty
C_7H_{16}	0.020%	0.025%
C_8H_{18}	0.036%	±0.000066 bar
C_9H_{20}	0.020%	0.200%
$C_{10}H_{22}$	0.020%	±0.000066 bar
$C_{11}H_{24}$	0.200%	
$C_{12}H_{26}$	0.200%	0.200%
$C_{13}H_{28}$	±0.0002 (gm/cc)	
$C_{14}H_{30}$	0.100%	±[0.0015P +0.000048] bar[a]
$C_{15}H_{32}$	0.100%	
$C_{16}H_{34}$	±0.00003 (gm/cc)	±[0.0015P +0.000048] bar[a]
$C_{17}H_{36}$	0.200%	
$C_{18}H_{38}$	0.100%	±[0.0015P +0.000048] bar[a]
$C_{19}H_{40}$	0.100%	±[0.0015P +0.000048] bar[a]
$C_{20}H_{42}$	0.200%	±[0.0015P +0.000048] bar[a]
$C_{22}H_{46}$		±[0.0015P +0.000048] bar[a]
$C_{23}H_{48}$	0.100%	
$C_{24}H_{50}$	0.100%	±[0.0015P +0.000048] bar[a]
$C_{28}H_{58}$	0.070%	±[0.0015P +0.000048] bar[a]
$C_{30}H_{62}$	0.200%	
$C_{36}H_{74}$	0.070%	
$C_{40}H_{82}$	0.200%	

[a] Uncertainty is pressure dependent and is given as ±[0.0015P +0.000048] bar, where P is pressure in bar.

Table 2
Coefficients in the correlations of Riazi and AlQaheem [32] given in Eq. (6).

Carbon number	a_1	a_2	a_3	b_1	b_2	b_3	c_1	c_2
C_1–C_{50}	−3.0337	0.3265	−0.0018060	−1.0097	−0.2056	0.001702	4.0519	−0.1216
C_{51}–C_{100}	0.9948	0.1581	−0.0006864	−2.5795	−0.1275	0.0008085	1.5701	−0.03715

In Eq. (6), $P_r^{vap} = (P^{vap}/P_C)$ and $T_r = (T/T_C)$. Coefficients a_1, a_2, a_3, b_1, b_2, b_3, c_1 and c_2 are given in Table 2. The r values for some hydrocarbons between C_2 and C_{40} are available in Riazi [9]. For other hydrocarbons up to C_{100}, the procedure recommended by Riazi and AlQaheem [32] has been used to estimate the value for r. Eq. (6) results in less than 2% deviation in vapor pressure predictions for the CN range shown in Table 2. Table A1 indicates n-alkanes for which the correlation of Riazi and AlQaheem [32] is used. For all the n-alkanes considered in our optimization, C_7–C_{100}, we ensure use of vapor pressure data points both for $T_r \leq 0.7$ and $T_r \geq 0.7$. This is to ensure the accuracy of vapor pressure predictions around T_r of 0.7, which is used in Pitzer's definition of ω in Eq. (7).

$$\omega = -\log_{10}\left[\frac{P_{SAT}}{P_C}\right]_{((T/T_C)=0.7)} - 1. \quad (7)$$

2.2. Optimization method

T_C, P_C, and ω are optimized considering reduction of

- average absolute deviation (AAD) in density predictions,
- AAD in vapor pressure predictions, and
- deviations of T_C and P_C from physical critical points,

while keeping smooth variations of T_C, P_C, and ω with respect to molecular weight (MW), and the consistency with Pitzer's definition for ω, Eq. (7). The minimization of AADs for both density and vapor pressure predictions can be challenging. A set of T_C, P_C, and ω that gives a minimum for the sum of the two types of AADs does not necessarily result in a minimum for each of the AADs. When a change in P_C decreases AAD in density predictions, it can increase AAD in vapor pressure predictions. For this reason, our optimization also considers that AAD in vapor pressure predictions should be similar to that in density predictions.

Minimization of the AADs can have many local minima, and it is unlikely that the global minimum always exists for this minimization. Smoothness of T_C, P_C, and ω with respect to MW is considered when the minimization needs an additional criterion due to multiple local minima close to each other.

2.2.1. Initialization

We optimize T_C, P_C, and ω using the exhaustive search method, for which initial estimates are provided using the solver function within the Excel software. The initialization using the Excel solver function starts with T_C, P_C, and ω from the correlations developed for n-alkanes by Gao et al. [33]. Predictions of vapor pressures and saturated liquid densities are sensitive to T_C and P_C, respectively [14]. Therefore, T_C and P_C are primarily used to reduce AADs in vapor pressure and density predictions. The initialization steps for a given n-alkane are as follows:

Step 1. AAD in vapor pressure predictions is reduced using T_C only.
Step 2. AAD in vapor pressure predictions is reduced using m only. The m parameter is defined in Eqs. (4) and (5).
Step 3. AAD in liquid density predictions is reduced using P_C only.
Step 4. The sum of AADs for vapor pressure and liquid density predictions is reduced using T_C and P_C.
Step 5. The sum of AADs for vapor pressure and liquid density predictions is reduced using T_C, P_C, and m.

Steps 1–5 are repeated until reduction of the AADs becomes marginal. During the iteration, we confirm that T_C, P_C, and m with respect to MW are smooth for 94 n-alkanes from C_7 to C_{100}. The values for T_C, P_C, and m that do not follow the smooth trends are replaced with values interpolated between the neighboring CNs.

The values for T_C and P_C initialized above are generally greater than physical values given in the literature. For example, the initialized critical point for C_{100} is (T_C, P_C) = (1094.0 K, 4.34 bar), and the physical critical point is (T_C, P_C) = (1038.2 K, 2.71 bar) [34]. The deviation from the physical values is reduced in the subsequent optimization using the exhaustive search method.

2.2.2. Exhaustive search for optimum T_C, P_C, and ω

An algorithm was developed for our optimization using the exhaustive search method. The algorithm allows for simultaneous adjustment of T_C, P_C, and m, unlike the initialization described in Section 2.2.1.

The exhaustive search method defines its search domain to be (−5%, +1%) from the initial value for T_C and (−8%, +2%) from the initial value for P_C for each n-alkane. This rectangular domain in T–P space is then discretized into 6000 grids allowing for a unit change of 0.1% in each of T_C and P_C. We use the asymmetric search domain with respect to the initial point in T and P directions. This is because we search for optimum values that are lower than the initial values set in Section 2.2.1.

For each set of T_C and P_C, we calculate m by minimizing AAD in vapor pressure predictions. In this optimization of m, we consider the consistency with Pitzer's definition of ω. For a given set of T_C, P_C, and m, the PR EOS can provide a saturation pressure at T_r of 0.7 (P_{SAT} in Eq. (7)). Eq. (7) can then give a value for ω. However, this ω value does not necessarily match another ω value that can be calculated from either Eq. (4) or Eq. (5) with the current m value. The consistency is satisfied when the absolute difference between these two ω values becomes smaller than a tolerance (e.g., 10^{-3}).

The resulting set of T_C, P_C, and m is then used to calculate AAD in liquid density predictions. The AADs in vapor pressure and liquid density predictions are recorded for 6000 sets of T_C, P_C, and m. Selection of the optimum set of T_C, P_C, and m for each n-alkane is, in general, based on the total of the AADs in vapor pressure and liquid density predictions. It is observed that the optimum set results in vapor pressure and liquid density AADs that are similar to each other. Smooth curves are usually observed for optimum T_C, P_C, and m with respect to MW. If a set of T_C, P_C, and m that gives the minimum AADs deviates from the overall trends, it is replaced by another set of T_C, P_C, and m while minimizing AADs.

3. Optimum T_C, P_C, m, and ω

The method discussed in Section 2 gives T_C, P_C, and m optimized for vapor pressure and liquid density predictions using the PR EOS for 94 n-alkanes from C_7 through C_{100}. Optimized values for ω are calculated using Eqs. (4) and (5). The final values for T_C, P_C, m, and ω are presented in Table A2 along with T_C, P_C, and ω based on the correlations of Gao et al. [33], which are given in Eqs. (8)–(10).

$$T_C = [6573.87 - 4680.77\exp(-0.1831(CN^{0.6667} - 2.08))]^{(1/1.276)} \quad (8)$$

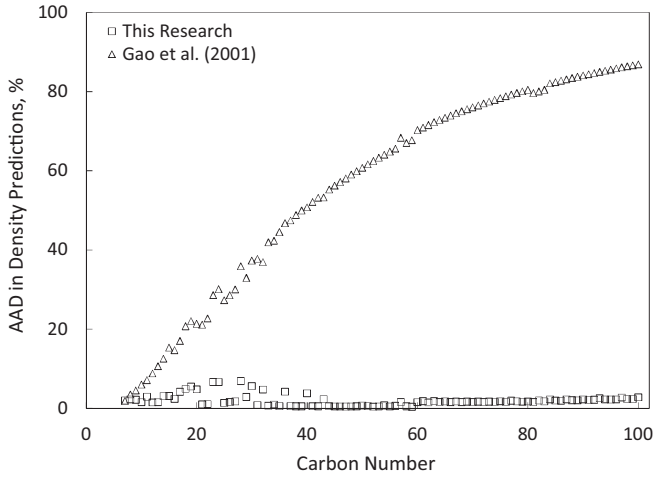

Fig. 2. Average absolute deviation (AAD) in density predictions for n-alkanes from C_7 to C_{100} using the correlations developed in this research and the correlations of Gao et al. [33].

$$P_C = 42.44\ \exp(-0.3757(\mathrm{CN}^{0.5684} - 1.8672)) \quad (9)$$

$$\omega = [3.212102 - 2.937628 \times \exp(-0.04699(\mathrm{CN}^{0.6667} - 2.08))]^{(1/0.6851)} \quad (10)$$

In the above equations, CN is carbon number. T_C and P_C are in K and bar, respectively. The accuracy (AAD) of the above correlations for T_C, P_C, and ω is 0.2, 0.8, and 0.4%, respectively, for n-alkanes from C_3 to C_{36}.

Use of our optimized T_C, P_C, and ω with the PR EOS gives significantly improved calculations of vapor pressure and liquid density for n-alkanes from C_7 to C_{100} as shown in Table A1. Using the optimized values, the AAD is 2.8% for 3583 density data points and 1.6% for 1525 vapor pressure data points. These data points include n-alkanes from C_7 to C_{100}. Figs. 2 and 3 present the comparisons of density and vapor pressure predictions using our optimized T_C, P_C, and ω with those using Eqs. (8)–(10). Using the optimized T_C, P_C, and ω, AADs for both density and vapor pressure predictions are consistently small for the wide range of CN from C_7 to C_{100}.

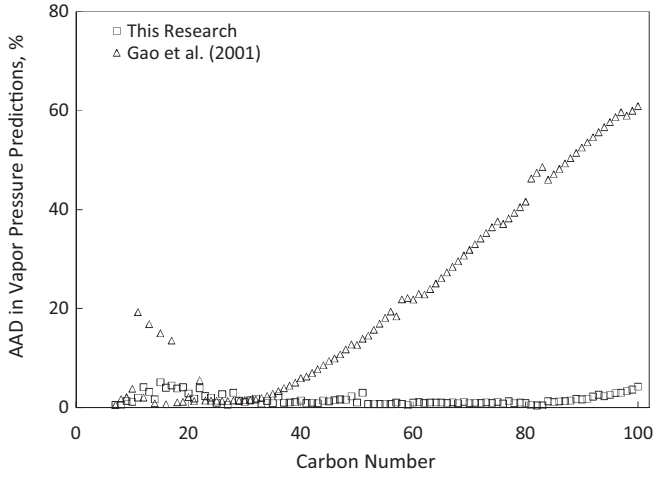

Fig. 3. Average absolute deviation (AAD) in vapor pressure predictions for n-alkanes from C_7 to C_{100} using the correlations developed in this research and the correlations of Gao et al. [33].

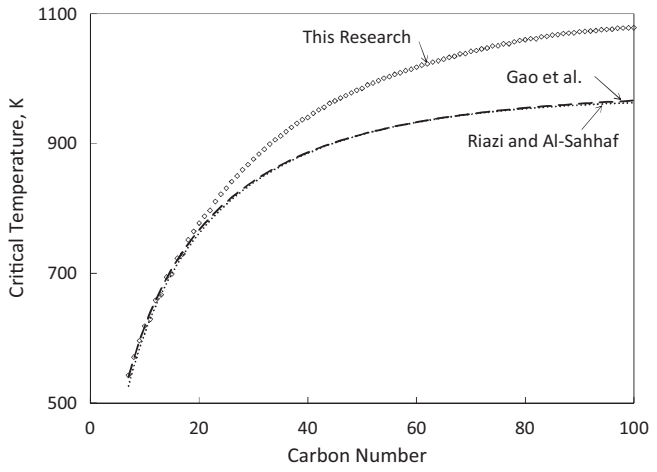

Fig. 4. Optimum critical temperature (T_C) developed for the PR EOS in this research, and the T_C correlations of Gao et al. [33] and Riazi and Al-Sahhaf [35].

A reason for the smaller variation of the AADs for CN greater than 40 is the relatively consistent T_r–P_r ranges and sources for the data used (see Table A1). When Eqs. (8)–(10) are used, AADs for density and vapor pressure predictions increase with CN. The AAD for C_{100} is 86.9% for density prediction and 60.9% for vapor pressure prediction when the correlations of Gao et al. [32], Eqs. (8)–(10), are used.

As mentioned before, the objective of our optimization is to develop T_C, P_C, and ω that give accurate phase behavior predictions for n-alkanes up to C_{100} using the PR EOS. That is, the values for T_C and P_C presented in Table A2 are not physical critical points. There are a few different proposals for T_C, P_C, and ω correlations for heavy n-alkanes in the literature. Gao et al. [33] developed correlations for T_C, P_C, and ω for n-alkanes up to C_{100}, which are given in Eqs. (8)–(10). Riazi and Al-Sahhaf [35] developed their correlations that are recommended for n-alkanes up to C_{20}. Although efforts have been made to minimize the deviation from physical values in our optimization (see Section 2), Figs. 4–6 show that T_C, P_C, and ω developed in this research deviate from values available in the literature. In these figures, Riazi and Al-Sahhaf's correlations are extrapolated up to C_{100}. Yaws [28] also gives values for T_C and P_C for n-alkanes, but they are not shown in Figs. 4–6 because their trends are not smooth at C_{30}.

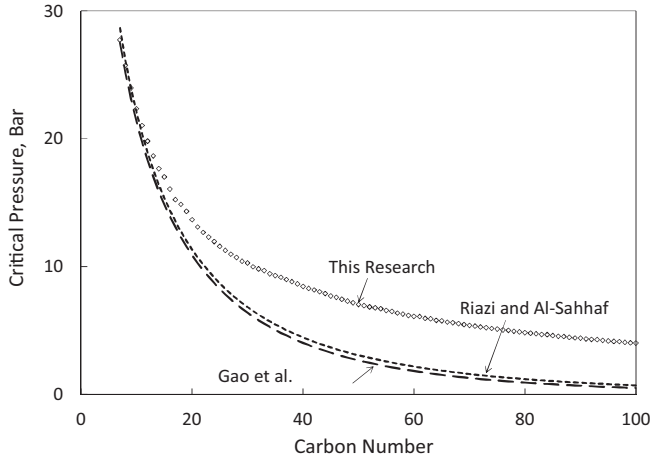

Fig. 5. Optimum critical pressure (P_C) developed for the PR EOS in this research, and the P_C correlations of Gao et al. [33] and Riazi and Al-Sahhaf [35].

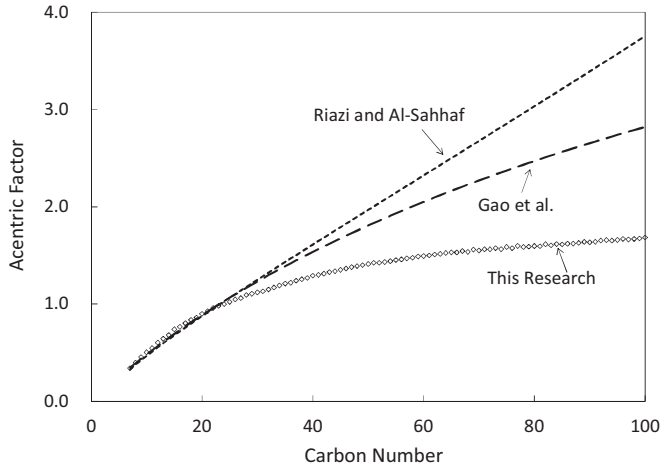

Fig. 6. Optimum acentric factor (ω) developed for the PR EOS in this research, and the ω correlations of Gao et al. [33] and Riazi and Al-Sahhaf [35].

Eqs. (11)–(13) present new correlations developed for T_C, P_C, and m using the optimized values given in Table A2. These correlations are recommended for use with the PR EOS only.

$$T_C = 1154.35 - 844.83[1.0 + 1.7557 \times 10^{-3}\,\mathrm{MW}]^{-2.0} \quad (11)$$

$$P_C = 559.93\,\mathrm{MW}^{-0.638} - 1.49 \quad (12)$$

$$m = 0.4707 + 2.4831\,\mathrm{MW}^{(-(39.933/\mathrm{MW}))} \quad (13)$$

In Eqs. (11)–(13), T_C is in K, P_C is in bar, and MW is in gm/mol. These correlations accurately represent the optimized T_C, P_C, and m. The R^2 values are 0.99975, 0.99970, and 0.99949 for T_C, P_C, and m, respectively. Maximum absolute deviations for Eqs. (11)–(13) are 7.35 K for n-$C_{15}H_{32}$, 0.24 bar for n-$C_{21}H_{64}$, and 0.0022 for n-$C_{31}H_{64}$, respectively. Standard deviations are 1.74 K for Eq. (11), 0.07 bar for Eq. (12), and 0.005 for Eq. (13). Eq. (11) shows an asymptotic value of 1154.35 K for T_C. An asymptote of 2.9538 for m can be found in Eq. (13). Eq. (12) gives P_C of 1.0 bar for MW of 4856 gm/mol, which is close to the MW of n-C_{347}.

Fig. 7 shows a sensitivity analysis for Eq. (11) in terms of AADs in density and vapor pressure predictions. The AADs here consider all data points (3583 density and 1525 vapor pressure data) for n-alkanes from C_7 to C_{100}. The AAD is 3.0% for density predictions and is 3.4% for vapor pressure predictions using Eqs. (11)–(13). The AAD in density predictions exhibit a monotonic trend with respect to T_C near the optimum values given by Eq. (11). Fig. 7 also indicates that vapor pressure predictions are more sensitive to T_C than density predictions. Eq. (11) gives a minimum in the density AAD and the total AAD.

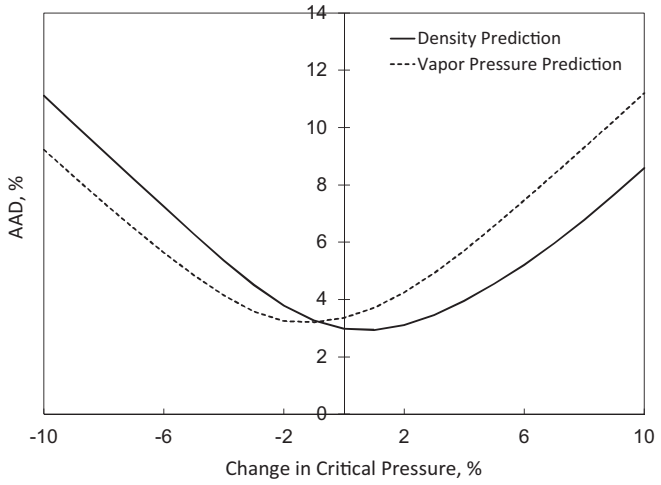

Fig. 8. Sensitivity of density and vapor pressure predictions to P_C around the optimum values given in Eq. (12). The 0% change in P_C corresponds to use of Eq. (12), which gives a minimum in the sum of the AADs in density and vapor pressure predictions.

Fig. 8 presents a similar sensitivity analysis for Eq. (12). The density AAD exhibits a minimum with a small positive change in P_C, while the vapor pressure AAD exhibits a minimum with a small negative change in P_C. Eq. (12) gives a minimum for the sum of the two AADs.

Fig. 9 shows the sensitivity of the AADs to the m parameter near the optimum values given in Eq. (13). The vapor pressure AAD is sensitive to the m parameter, but the density AAD is nearly constant for ±10% changes from Eq. (13). Eq. (13) gives a minimum for the vapor pressure AAD and the total AAD. Figs. 7–9 also show that density predictions are more sensitive to P_C than to T_C and the m parameter.

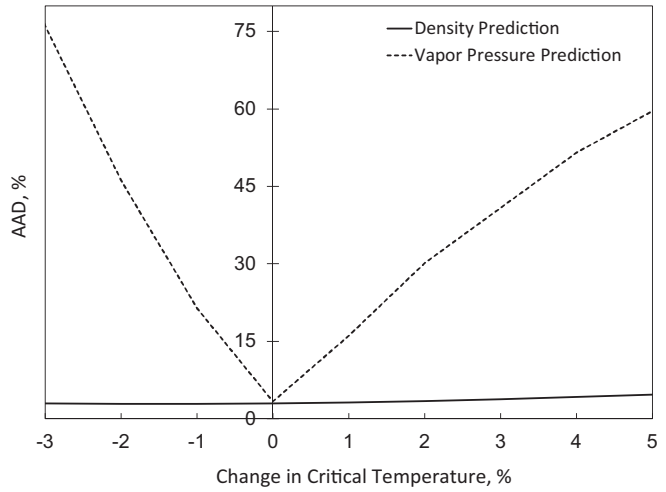

Fig. 7. Sensitivity of density and vapor pressure predictions to T_C around the optimum values given in Eq. (11). The 0% change in T_C corresponds to use of Eq. (11), which gives a minimum in the sum of the AADs in density and vapor pressure predictions.

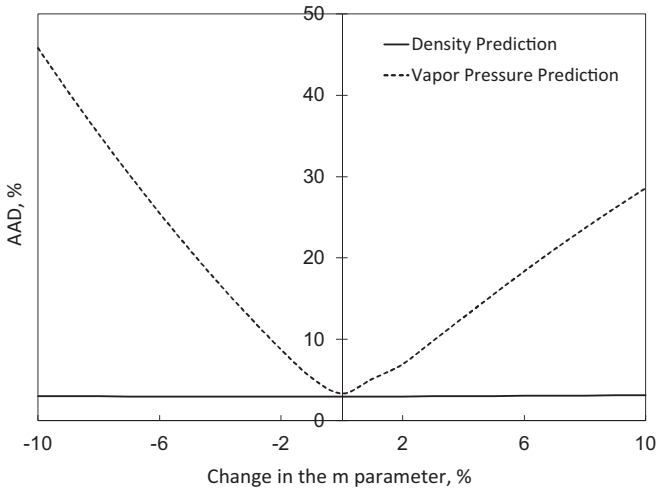

Fig. 9. Sensitivity of density and vapor pressure predictions to the m parameter around the optimum values given in Eq. (13). The 0% change in m corresponds to use of Eq. (13), which gives a minimum in the sum of the AADs in density and vapor pressure predictions.

Table 3
AADs in density predictions for n-alkane mixtures using the PR EOS. AADs using Eqs. (11)–(13) developed in this research are compared to those using Eqs. (8)–(10) of Gao et al. [33].

Components	No. of data	Ref.	AAD This research	AAD Gao et al.
Heptane (C_7) + octane (C_8)	11	[36]	0.3	1.7
Heptane (C_7) + nonane (C_9)	11	[36]	0.7	2.9
Heptane (C_7) + decane (C_{10})	11	[36]	1.2	4.1
Heptane (C_7) + undecane (C_{11})	11	[36]	0.6	5.3
Heptane (C_7) + dodecane (C_{12})	10	[36]	1.7	6.5
Heptane (C_7) + hexadecane (C_{16})	11	[36]	3.1	12.6
Octane (C_8) + nonane (C_9)	11	[36]	0.9	3.8
Octane (C_8) + decane (C_{10})	11	[36]	1.2	4.8
Octane (C_8) + undecane (C_{11})	11	[36]	0.7	5.9
Octane (C_8) + dodecane (C_{12})	11	[36]	1.9	7.3
Octane (C_8) + hexadecane (C_{16})	11	[36]	3.2	12.8
Nonane (C_9) + decane (C_{10})	11	[36]	1.4	5.6
Nonane (C_9) + undecane (C_{11})	11	[36]	0.9	6.7
Nonane (C_9) + dodecane (C_{12})	11	[36]	1.9	7.8
Nonane (C_9) + hexadecane (C_{16})	11	[36]	3.3	15.2
Decane (C_{10}) + undecane (C_{11})	11	[36]	1.3	7.6
Decane (C_{10}) + dodecane (C_{12})	11	[36]	2.3	8.7
Decane (C_{10}) + hexadecane (C_{16})	11	[36]	3.4	13.5
Undecane (C_{11}) + dodecane (C_{12})	11	[36]	1.8	9.5
Undecane (C_{11}) + hexadecane (C_{16})	11	[36]	3.0	14.1
Dodecane (C_{12}) + hexadecane (C_{16})	11	[36]	3.7	14.7
Decane (C_{10}) + eicosane (C_{20})	24	[37]	4.2	18.0
Decane (C_{10}) + docosane (C_{22})	20	[37]	4.6	20.7
Decane (C_{10}) + tetracosane (C_{24})	16	[37]	4.9	23.5
Decane (C_{10}) + docosane (C_{22}) + tetracosane (C_{24})	23	[37]	4.8	21.8

4. Application of optimized critical parameters to mixtures

In Section 3, we developed a new set of critical parameters for the PR EOS that can accurately predict liquid densities and vapor pressures of n-alkanes up to C_{100}. This section is to show that the PR EOS with the critical parameters developed also improves phase behavior predictions for mixtures. We first demonstrate improved phase behavior predictions for various n-alkane mixtures. Application of our critical parameters is then presented for characterization of 25 different reservoir oils. All phase behavior calculations in this section use the PR EOS with the van der Waals mixing rules, and zero binary interaction between hydrocarbons.

4.1. Phase behavior predictions for n-alkane mixtures

We make comparisons between the PR EOS with our correlations for critical parameters [i.e., Eqs. (10)–(12)] and the PR EOS with the correlations of Gao et al. [33] [i.e., Eqs. (8)–(10)]. No attempts are made to adjust parameters to obtain a better match between experimental data and predictions.

Table 3 shows use of our correlations gives improved accuracy for density predictions for various n-alkane mixtures. AADs in density predictions become greater for heavier hydrocarbons when the correlations of Gao et al. [33] are used. Use of our correlations for the PR EOS exhibits consistently small AADs in density predictions for all mixtures studied.

The two sets of the correlations are also compared in terms of bubble point pressure predictions for six different mixtures, C_1–C_{16}, C_1–C_{20}, C_2–C_{16}, C_2–C_{20}, C_2–C_{22}, and C_2–C_{24}. For C_2–C_{22} and C_2–C_{24} mixtures, bubble point pressures at two different temperatures are considered for the comparisons. Predictions of bubble and dew points are compared for three n-alkane binaries C_6–C_{16}, C_6–C_{24}, and C_6–C_{36}. As shown in Figs. 10–20, use of our correlations gives more accurate predictions for bubble and dew points pressures for most of the mixtures studied. Our correlations ensure that bubble point and dew point pressures near the end points (i.e., 0.0 and 1.0 on the *x*-axis) of the figures are accurately predicted using the PR EOS.

Deviations from experimental data are observed for middle-range mixing ratios. Such deviations are attributed mainly to the van der Waals mixing rules used to estimate the attraction and covolume parameters for mixtures. The deviations can be significantly improved if a binary interaction parameter is adjusted for each n-alkane binary. We developed the optimized critical parameters considering their application for characterization of reservoir oils. In reservoir oil characterization, the main challenge comes from uncertainties in properties and amounts of non-identifiable components. Adjustment of binary interaction parameters for such a case can result in physically absurd predictions [10]. That is, we do not show adjustment of binary interaction parameters to fit EOS predictions to data in this research.

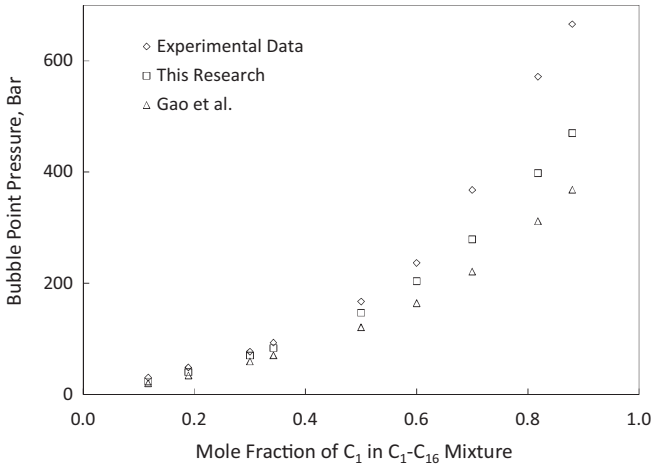

Fig. 10. Comparison of bubble point pressure predictions with experimental data (Peter et al. [38]) for C_1–C_{16} mixtures at 300 K. For the predictions, the PR EOS is used with the critical parameters developed in this research and those by Gao et al. [33].

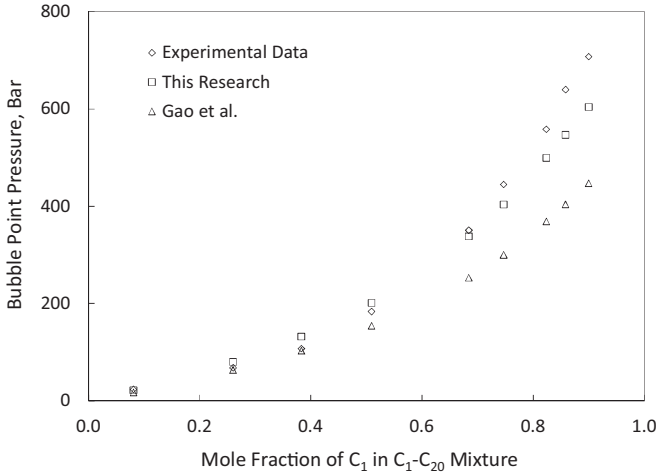

Fig. 11. Comparison of bubble point pressure predictions with experimental data [38] for C_1–C_{20} mixtures at 363.15 K. For the predictions, the PR EOS is used with the critical parameters developed in this research and those by Gao et al. [33].

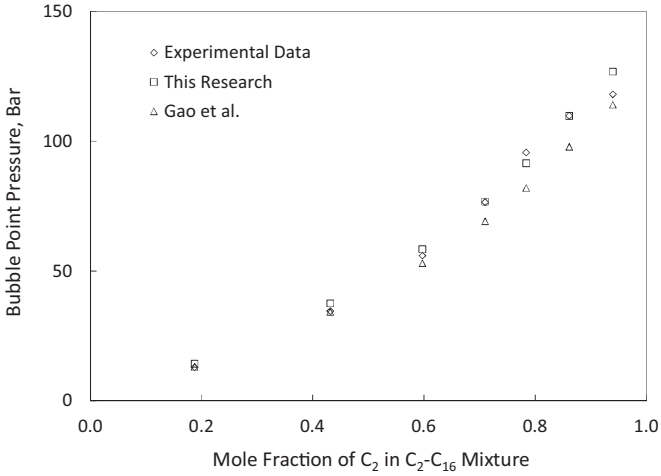

Fig. 12. Comparison of bubble point pressure predictions with experimental data [38] for C_2–C_{16} mixtures at 363.15 K. For the predictions, the PR EOS is used with the critical parameters developed in this research and those by Gao et al. [33].

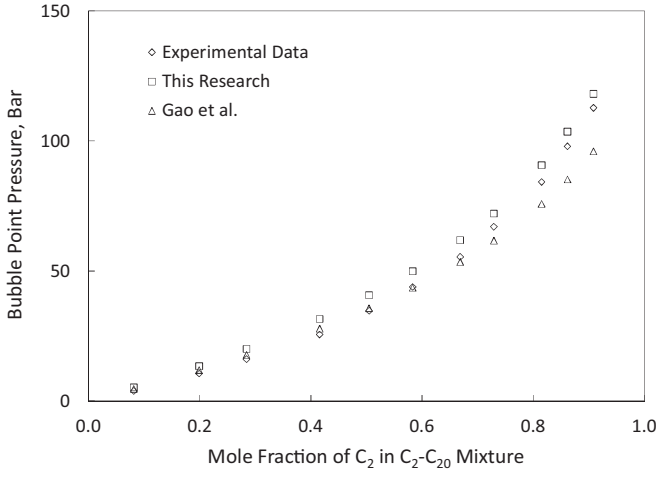

Fig. 13. Comparison of bubble point pressure predictions with experimental data [38] for C_2–C_{20} mixtures at 350 K. For the predictions, the PR EOS is used with the critical parameters developed in this research and those by Gao et al. [33].

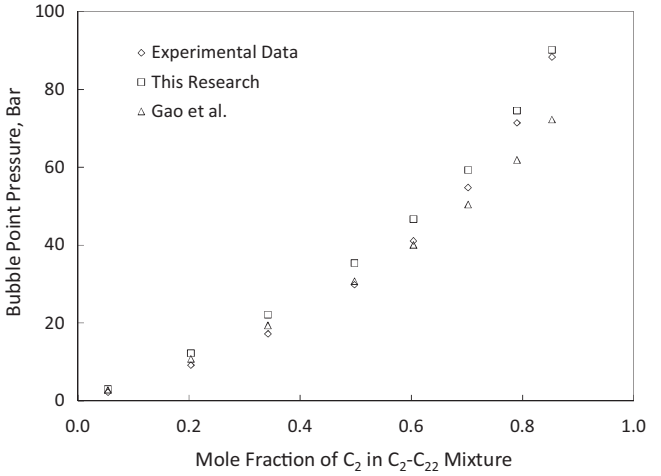

Fig. 14. Comparison of bubble point pressure predictions with experimental data [38] for C_2–C_{22} mixtures at 340 K. For the predictions, the PR EOS is used with the critical parameters developed in this research and those by Gao et al. [33].

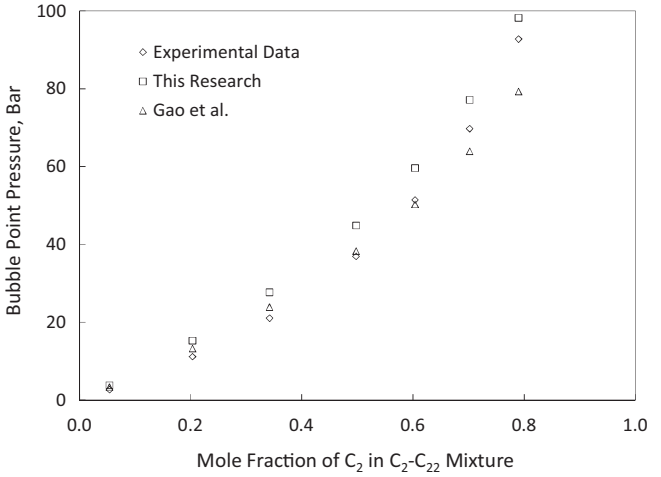

Fig. 15. Comparison of bubble point pressure predictions with experimental data [39] for C_2–C_{22} mixtures at 360 K. For the predictions, the PR EOS is used with the critical parameters developed in this research and those by Gao et al. [33].

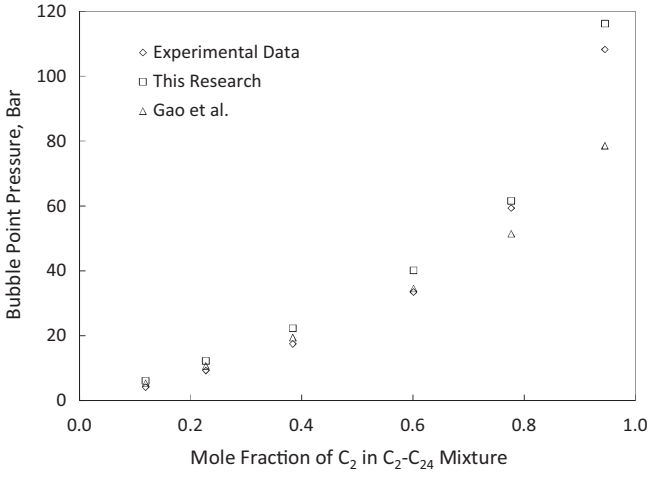

Fig. 16. Comparison of bubble point pressure predictions with experimental data [38] for C_2–C_{24} mixtures at 330 K. For the predictions, the PR EOS is used with the critical parameters developed in this research and those by Gao et al. [33].

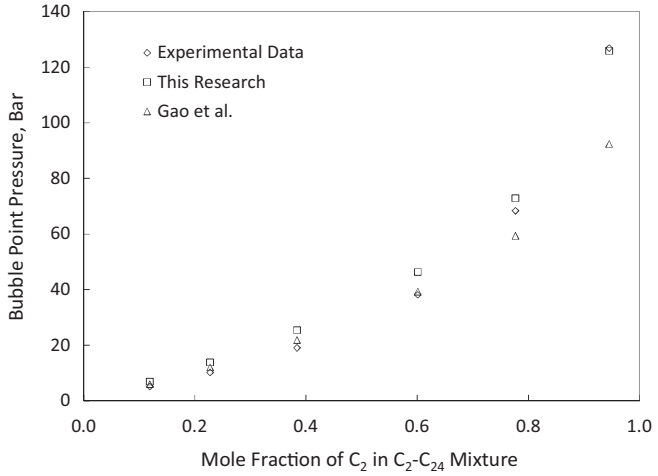

Fig. 17. Comparison of bubble point pressure predictions with experimental data [38] for C_2–C_{24} mixtures at 340 K. For the predictions, the PR EOS is used with the critical parameters developed in this research and those by Gao et al. [33].

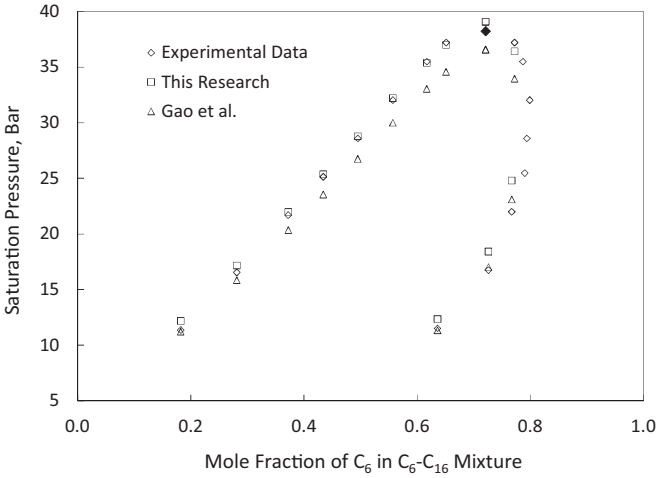

Fig. 18. Comparison of bubble and dew point predictions with experimental data [40] for C_6–C_{16} mixture at 623 K. The critical point is given as ♦. For the predictions, the PR EOS is used with the critical parameters developed in this research and those by Gao et al. [33].

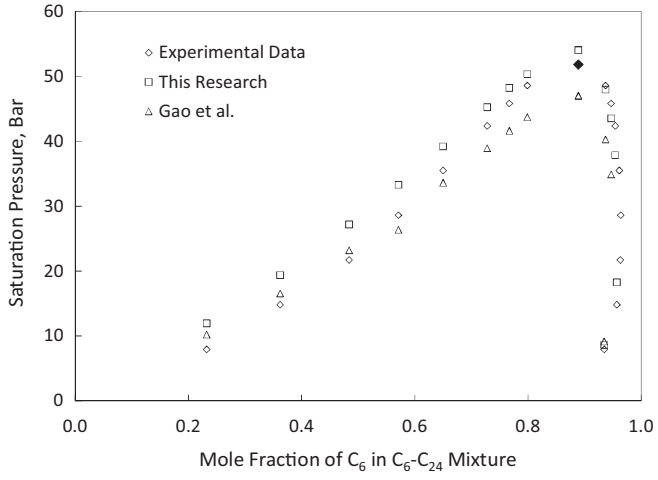

Fig. 19. Comparison of bubble and dew point predictions with experimental data [41] for C_6–C_{24} mixture at 622.9 K. The critical point is given as ♦. For the predictions, the PR EOS is used with the critical parameters developed in this research and those by Gao et al. [33].

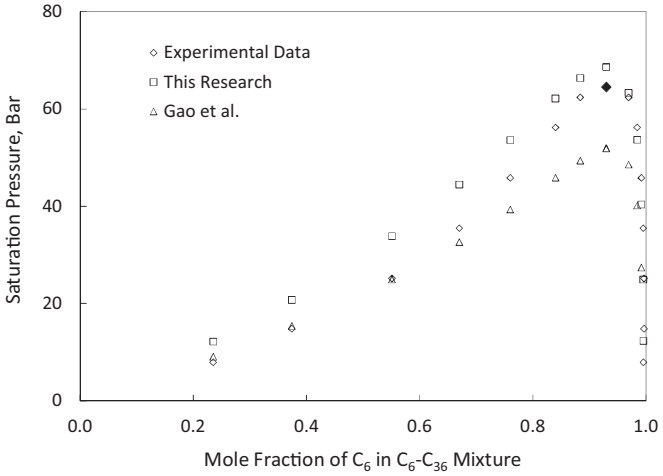

Fig. 20. Comparison of bubble and dew point predictions with experimental data [41] for C_6–C_{36} mixture at 621.8 K. The critical point is given as ♦. For the predictions, the PR EOS is used with the critical parameters developed in this research and those by Gao et al. [33].

4.2. Density prediction for reservoir oils

Different reservoir oils have different distributions of CN groups and PNA components within a given CN group. Even for a given reservoir oil, the concentrations of PNA components likely vary with CN. Characterization of heavy oils is more difficult than that of conventional oils because heavy oils contain a larger amount of heavy fractions, for which CN and PNA distributions are highly uncertain.

In a typical fluid characterization using an EOS, a distribution of CN groups is estimated based on composition analysis data available. Once a CN group distribution is specified, critical parameters are assigned to each CN group. Correlations for critical parameters proposed in the literature are generic in that they do not explicitly consider the concentrations of PNA components. Use of these generic correlations is unsuitable for heavy oil characterization because a heavier CN group can have a wider variety of compounds in it.

A potential method to address the uncertainties is to consider a PNA distribution in a reservoir oil as perturbation from n-alkane mixtures. The critical parameters developed in this research for a homologous series of n-alkanes can serve as a well-defined reference for the perturbation consideration. Since T_C and P_C for N and A components are in general greater than those for P components within a given CN group, T_C and P_C for n-alkanes developed in this research provide the lower bounds of critical parameters for pseudo components for actual oils.

Quiñones-Cisneros et al. [27,42,43] proposed a novel fluid characterization method. In their method, P_C for a pseudo component is expressed as $P_{Ci} = f \times P_{CPi}$, where i is a component index, P_{CP} is P_C for paraffinic components, and f is a perturbation factor that represents deviation from P_{CP}. So, the f factor is 1.0 for P_{CPi}.

In this section, we apply the critical parameters developed in this research for characterizing 25 reservoir oils (Table 4) on the basis of Quiñones-Cisneros et al.'s characterization method. Measured saturation pressures are used to adjust P_C through the perturbation factor f as in Quiñones-Cisneros et al. [27,42,43]. No other parameters are adjusted. Density predictions are then compared with experimental data.

The characterization steps given below are applied to 25 different reservoir oils presented in Table 4.

Step 1. Composition. Heavy fractions are split into detailed components using a chi-square distribution. The detailed components

Table 4
Comparisons of density predictions using the correlations developed in this research [Eqs. (11)–(13)] and those using the correlations of Quiñones-Cisneros et al. [Eqs. (14)–(16)]. Volume shift parameters are not used for these comparisons.

Oils	API gravity (calculated)	Molecular weight	No. of data	Ref.	This research		Quiñones-Cisneros et al.	
					Perturbation factor	AAD [%]	Perturbation factor	AAD [%]
Oil-1	60.18	86.57	13	[44]	1.1201	4.8	1.2655	7.8
Oil-6	55.73	83.31	20	[45]	1.2639	12.0	1.4330	14.9
Oil-2	47.63	89.83	11	[44]	1.3033	13.3	1.4537	16.2
Oil-7	47.09	113.60	20	[45]	1.2064	7.2	1.3515	10.0
Light oil	43.68	105.26	7	[46]	1.2158	5.8	1.3424	7.5
Oil-3	40.46	87.80	5	[44]	1.4226	18.2	1.6044	22.1
Fluid-1	35.73	124.57	8	[6]	1.3327	12.6	1.4845	16.6
Oil-6	35.67	118.18	5	[44]	1.2828	7.7	1.4482	11.7
Oil-3	34.24	114.65	12	[27]	1.4056	15.7	1.5612	18.9
Oil-1	34.04	123.79	8	[45]	1.3869	12.5	1.5594	16.1
Oil-4	33.35	114.57	6	[44]	1.3827	14.6	1.5497	19.0
Oil-7	29.24	159.99	16	[44]	1.2658	5.0	1.4123	9.4
Oil-5	28.90	130.55	3	[44]	1.3984	14.3	1.5610	18.8
Oil[b]	22.60[a]	296.90	13		1.0697	10.2	1.1659	8.2
Oil-4	25.70	167.03	11	[27]	1.4204	14.0	1.5624	16.9
Oil-8	24.25	182.05	16	[44]	1.3625	9.3	1.5149	13.6
Oil-1	20.81	170.59	16	[43]	1.2869	7.3	1.4230	10.9
Oil-5	20.19	240.24	15	[27]	1.3031	1.9	1.4217	3.7
Oil-G	17.01	237.92	12	[48]	1.5368	17.9	1.7087	23.1
Oil-H	13.84	232.17	15	[48]	1.3395	2.1	1.4655	4.6
Oil-6	13.38	377.88	13	[43]	1.0126	21.6	1.0943	20.3
Oil-5	11.98	422.94	13	[43]	1.1124	14.7	1.1970	13.7
Oil-7	11.63	431.59	12	[42]	1.0854	16.9	1.1671	15.9
Heavy oil	10.00[a]	421.35	8	[47]	1.6511	24.9	1.7762	26.4
Oil-8	9.50	443.06	13	[42]	1.1255	15.1	1.2089	14.2

Total number of data = 291.
Overall AAD for this research = 11.20%.
Overall AAD for Quiñones-Cisneros et al. = 13.48%.
[a] API as reported.
[b] This is an actual oil, but the source is not mentioned due to confidentiality.

are then grouped into 10 components consisting of N_2, CO_2, C_1, C_{2-3}, C_4, C_5, and four heavy pseudo components.

Step 2. Critical parameters. For the well-defined components (i.e., N_2, CO_2, and C_1–C_5), physical critical parameters available in the literature are used. For the four pseudo components, two sets of correlations are used; Eqs. (11)–(13) developed in this research and the correlations of Quiñones-Cisneros et al. [42] as given by

$$T_C = -423.587 + 210.152 \ln(\mathrm{MW}) \quad (14)$$

$$P_C = \exp(9.67283 - 4.05288\,\mathrm{MW}^{0.1}) \quad (15)$$

$$\omega = \exp\left(8.50471 - \frac{15.1665}{\mathrm{MW}^{0.1}}\right) \quad (16)$$

Step 3. Perturbation of P_C. Adjust the perturbation factor f to match the experimental saturation pressure at the reservoir temperature.

For all reservoir oils characterized, binary interaction parameters between non-hydrocarbon and hydrocarbon components are 0.02 for N_2–C_1, 0.06 for N_2–C_{2-3}, 0.08 for N_2–$C_{i>3}$, 0.12 for CO_2–C_1, and 0.15 for CO_2–$C_{i>1}$ [42]. Volume-shift parameters are zero for all components. In the above, two fluid models are created for each of 25 reservoir oils; i.e., one using Eqs. (11)–(13) and the other using Eqs. (14)–(16) for T_C, P_C, and ω. Eqs. (14) and (16) are generic correlations that do not consider the PNA distribution, while Eq. (15) is the correlation for P_{CP} proposed by Quiñones-Cisneros et al. [42]. The two fluid models are compared in terms of density predictions for each of the reservoir oils studied (Table 4).

Table 4 lists the resulting perturbation factors for the 25 reservoir oils. The critical parameters developed in this research result in systematically reduced perturbation required to match saturation pressures. All the calculated perturbation factors are found to be greater than 1.0 using Eqs. (11)–(13). This observation is consistent with the fundamental concept of the perturbation; i.e., the perturbation factor represents deviation from P_{CP}, and P_C is lower for the P components than for the N and A components within a given CN group. The variation of the resulting perturbation factors is small for oils lighter than 25°API. A wider variation of the resulting perturbation factors is observed for heavier oils, which likely results from higher uncertainties in heavier oils' compositions.

Table 4 lists AADs in density predictions for the 25 reservoir oils using Eqs. (11)–(13) developed in this research and Eqs. (14)–(16) taken from Quiñones-Cisneros et al. [42]. As shown in Fig. 21, use of Eqs. (11)–(13) results in more accurate density predictions for most of the reservoir oils studied. The correlations developed in this

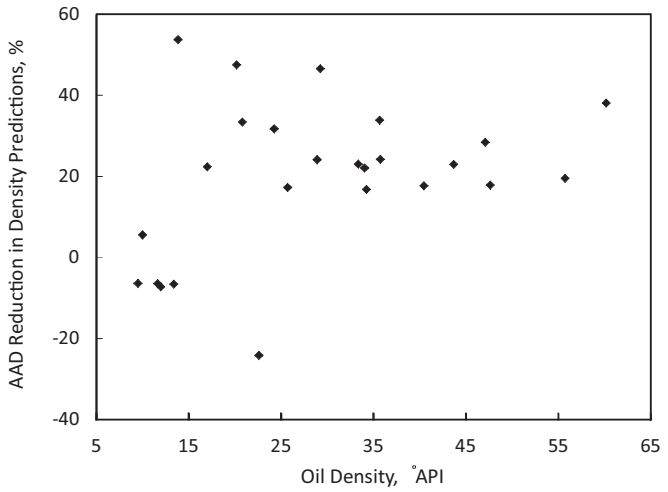

Fig. 21. AAD reduction in density predictions for 25 different reservoir oils listed in Table 3. AAD reduction in density predictions is defined as AAD using Eqs. (14)–(16) less AAD using Eqs. (11)–(13) divided by AAD using Eqs. (14)–(16).

Table A1
Sources and T–P ranges of data used for optimizing T_C, P_C, and ω, and AADs in density and vapor pressure predictions. AADs using optimum T_C, P_C, and ω developed in this research are compared to those using the correlations of Gao et al. [33].

n-Alkanes	Density data				AAD liquid density, %		Vapor pressure data			AAD vapor pressure, %	
	Source	No. of data	T_r range	P_r range	This research	Gao et al. [33]	Source	No. of data	T_r range	This research	Gao et al. [33]
C_7H_{16}	[49,50]	214	0.43–1.06	0.01–180.32	2.0	1.9	[52,61]	35	0.69–0.95	0.5	0.5
C_8H_{18}	[51,52]	54	0.52–1.05	0.52–1.05	2.3	3.5	[52,62]	27	0.53–0.95	0.5	1.7
C_9H_{20}	[49,50]	212	0.39–0.98	0.39–0.98	2.2	4.5	[52]	12	0.54–0.91	1.3	2.1
$C_{10}H_{22}$	[53,54]	131	0.48–0.98	0.48–0.98	1.5	6.0	[52,62]	28	0.50–0.92	1.1	3.8
$C_{11}H_{24}$	[28,49]	90	0.48–0.91	0.48–0.91	2.9	7.1	[32]	10	0.60–0.90	2.0	19.3
$C_{12}H_{26}$	[28,49]	170	0.48–0.79	0.48–0.79	1.5	8.8	[52]	14	0.53–0.93	4.1	2.0
$C_{13}H_{28}$	[28,55]	170	0.46–0.79	0.46–0.79	1.5	10.6	[32]	10	0.60–0.90	3.2	16.9
$C_{14}H_{30}$	[28,56]	80	0.42–0.79	0.42–0.79	3.1	12.5	[63]	20	0.60–0.79	1.6	0.9
$C_{15}H_{32}$	[28,57]	162	0.42–0.79	0.42–0.79	3.1	15.3	[32]	10	0.59–0.90	5.1	15.0
$C_{16}H_{34}$	[28,57]	193	0.43–0.78	0.43–0.78	2.4	14.7	[63]	19	0.55–0.80	4.0	0.7
$C_{17}H_{36}$	[28,49]	80	0.44–0.79	0.44–0.79	4.2	17.0	[32]	10	0.59–0.89	4.5	13.5
$C_{18}H_{38}$	[28,58]	123	0.42–0.88	0.42–0.88	5.0	20.7	[63]	20	0.60–0.88	3.8	1.1
$C_{19}H_{40}$	[28,58]	119	0.41–0.88	0.41–0.88	5.5	22.0	[63]	20	0.59–0.88	4.1	1.2
$C_{20}H_{42}$	[28,49]	70	0.48–0.87	0.48–0.87	4.8	21.4	[63]	20	0.59–0.87	2.8	2.1
$C_{21}H_{44}$	[28]	20	0.59–0.78	0.59–0.78	1.0	21.1	[32]	20	0.59–0.78	1.8	1.3
$C_{22}H_{46}$	[28]	20	0.59–0.77	0.59–0.77	1.1	22.7	[63]	22	0.57–0.88	3.9	5.5
$C_{23}H_{48}$	[28,59]	110	0.41–0.78	0.41–0.78	6.7	28.6	[32]	20	0.59–0.78	2.3	1.4
$C_{24}H_{50}$	[28,59]	105	0.41–0.77	0.41–0.77	6.6	30.1	[63]	20	0.59–0.77	2.0	1.4
$C_{25}H_{52}$	[28]	20	0.59–0.77	0.59–0.77	1.3	27.3	[32]	20	0.59–0.77	1.0	1.4
$C_{26}H_{54}$	[28]	20	0.59–0.77	0.59–0.77	1.6	28.6	[32]	20	0.59–0.77	2.7	1.3
$C_{27}H_{56}$	[28]	20	0.59–0.77	0.59–0.77	1.7	30.0	[32]	20	0.59–0.77	0.6	1.3
$C_{28}H_{58}$	[28,60]	101	0.41–0.86	0.41–0.86	6.9	35.8	[63]	20	0.58–0.86	3.0	1.4
$C_{29}H_{60}$	[28]	20	0.58–0.86	0.58–0.86	2.9	32.9	[32]	20	0.58–0.86	1.4	1.4
$C_{30}H_{62}$	[28,36]	70	0.43–0.86	0.43–0.86	5.6	37.3	[32]	20	0.58–0.86	1.1	1.5
$C_{31}H_{64}$	[28]	20	0.58–0.85	0.58–0.85	0.8	37.7	[32]	20	0.58–0.85	1.4	1.5
$C_{32}H_{66}$	[28]	19	0.59–0.85	0.59–0.85	4.7	36.9	[32]	19	0.59–0.85	1.8	1.6
$C_{33}H_{68}$	[28]	19	0.59–0.84	0.59–0.84	0.7	41.9	[32]	19	0.59–0.84	0.8	1.9
$C_{34}H_{70}$	[28]	19	0.59–0.84	0.59–0.84	1.0	42.3	[32]	19	0.59–0.84	1.3	2.3
$C_{35}H_{72}$	[28]	19	0.59–0.84	0.59–0.84	0.6	44.5	[32]	19	0.59–0.84	0.9	2.8
$C_{36}H_{74}$	[28,60]	83	0.40–0.85	0.40–0.85	4.2	46.8	[32]	18	0.60–0.85	2.3	3.3
$C_{37}H_{76}$	[28]	19	0.57–0.82	0.57–0.82	0.6	47.4	[32]	17	0.60–0.82	0.9	3.9
$C_{38}H_{78}$	[28]	18	0.60–0.84	0.60–0.84	0.5	48.8	[32]	18	0.60–0.84	1.0	4.4
$C_{39}H_{80}$	[28]	18	0.59–0.83	0.59–0.83	0.5	50.0	[32]	18	0.59–0.83	1.1	5.0
$C_{40}H_{82}$	[28,49]	58	0.45–0.84	0.45–0.84	3.8	50.8	[32]	17	0.61–0.84	1.4	11.3
$C_{41}H_{84}$	[28]	18	0.59–0.83	0.59–0.83	0.5	52.1	[32]	17	0.61–0.83	0.9	13.3
$C_{42}H_{86}$	[28]	18	0.59–0.83	0.59–0.83	0.5	53.2	[32]	17	0.61–0.83	1.0	13.8
$C_{43}H_{88}$	[28]	18	0.59–0.83	0.59–0.83	2.3	53.2	[32]	17	0.61–0.83	0.8	14.4
$C_{44}H_{90}$	[28]	17	0.60–0.83	0.60–0.83	0.6	55.2	[32]	17	0.60–0.83	1.4	15.0
$C_{45}H_{92}$	[28]	17	0.60–0.83	0.60–0.83	0.5	56.2	[32]	17	0.60–0.83	1.2	15.6
$C_{46}H_{94}$	[28]	17	0.60–0.83	0.60–0.83	0.5	57.2	[32]	16	0.62–0.83	1.5	15.8
$C_{47}H_{96}$	[28]	17	0.61–0.83	0.61–0.83	0.5	58.1	[32]	16	0.62–0.83	1.6	16.5
$C_{48}H_{98}$	[28]	17	0.60–0.82	0.60–0.82	0.5	59.0	[32]	16	0.61–0.82	1.6	17.3
$C_{49}H_{100}$	[28]	17	0.60–0.82	0.60–0.82	0.5	59.9	[32]	16	0.61–0.82	2.3	18.1
$C_{50}H_{102}$	[28]	17	0.60–0.83	0.60–0.83	0.7	60.7	[32]	16	0.62–0.83	1.0	17.8
$C_{51}H_{104}$	[28]	17	0.60–0.82	0.60–0.82	0.6	61.6	[32]	16	0.61–0.82	3.0	18.9
$C_{52}H_{106}$	[28]	16	0.61–0.82	0.61–0.82	0.4	62.5	[32]	15	0.62–0.82	0.7	19.2
$C_{53}H_{108}$	[28]	16	0.61–0.82	0.61–0.82	0.5	63.3	[32]	15	0.62–0.82	0.7	20.3
$C_{54}H_{110}$	[28]	16	0.61–0.82	0.61–0.82	0.7	64.1	[32]	15	0.62–0.82	0.7	21.3
$C_{55}H_{112}$	[28]	16	0.61–0.82	0.61–0.82	0.5	64.8	[32]	15	0.62–0.82	0.7	22.4
$C_{56}H_{114}$	[28]	16	0.61–0.82	0.61–0.82	0.6	65.6	[32]	15	0.62–0.82	0.7	23.5
$C_{57}H_{116}$	[28]	16	0.63–0.90	0.63–0.90	1.6	68.3	[32]	16	0.63–0.90	1.0	22.2
$C_{58}H_{118}$	[28]	16	0.61–0.81	0.61–0.81	0.5	67.0	[32]	15	0.62–0.81	0.7	25.6
$C_{59}H_{120}$	[28]	16	0.61–0.81	0.61–0.81	0.4	67.7	[32]	15	0.63–0.81	0.5	26.8
$C_{60}H_{122}$	[28]	16	0.62–0.90	0.62–0.90	1.5	70.2	[32]	16	0.62–0.90	1.0	25.2
$C_{61}H_{124}$	[28]	16	0.62–0.90	0.62–0.90	1.8	70.9	[32]	16	0.62–0.90	1.1	26.2
$C_{62}H_{126}$	[28]	16	0.62–0.90	0.62–0.90	1.5	71.5	[32]	16	0.64–0.90	0.9	27.3
$C_{63}H_{128}$	[28]	15	0.64–0.90	0.64–0.90	1.8	72.2	[32]	15	0.64–0.90	1.0	27.0
$C_{64}H_{130}$	[28]	15	0.64–0.90	0.64–0.90	1.6	72.8	[32]	15	0.64–0.90	1.0	28.0
$C_{65}H_{132}$	[28]	15	0.64–0.89	0.64–0.89	1.8	73.4	[32]	15	0.64–0.89	1.0	29.0
$C_{66}H_{134}$	[28]	15	0.64–0.89	0.64–0.89	1.6	73.9	[32]	15	0.64–0.89	0.9	30.0
$C_{67}H_{136}$	[28]	15	0.64–0.89	0.64–0.89	1.7	74.5	[32]	15	0.64–0.89	1.1	31.1
$C_{68}H_{138}$	[28]	15	0.64–0.89	0.64–0.89	1.6	75.0	[32]	15	0.64–0.89	0.8	32.1
$C_{69}H_{140}$	[28]	15	0.64–0.89	0.64–0.89	1.7	75.5	[32]	15	0.64–0.89	1.1	33.2
$C_{70}H_{142}$	[28]	15	0.64–0.89	0.64–0.89	1.6	76.0	[32]	15	0.64–0.89	0.9	34.2
$C_{71}H_{144}$	[28]	15	0.64–0.89	0.64–0.89	1.7	76.5	[32]	15	0.64–0.89	1.0	35.3
$C_{72}H_{146}$	[28]	15	0.63–0.89	0.63–0.89	1.6	77.0	[32]	15	0.63–0.89	0.9	36.3
$C_{73}H_{148}$	[28]	15	0.63–0.89	0.63–0.89	1.7	77.4	[32]	15	0.63–0.89	1.0	37.4
$C_{74}H_{150}$	[28]	15	0.63–0.89	0.63–0.89	1.6	77.9	[32]	15	0.63–0.89	0.9	38.4
$C_{75}H_{152}$	[28]	15	0.63–0.89	0.63–0.89	1.8	78.3	[32]	15	0.63–0.89	1.1	39.5
$C_{76}H_{154}$	[28]	15	0.63–0.88	0.63–0.88	1.6	78.8	[32]	15	0.65–0.88	0.8	40.6

Table A1 (*Continued*)

n-Alkanes	Density data				AAD liquid density, %		Vapor pressure data			AAD vapor pressure, %	
	Source	No. of data	T_r range	P_r range	This research	Gao et al. [33]	Source	No. of data	T_r range	This research	Gao et al. [33]
$C_{77}H_{156}$	[28]	15	0.63–0.89	0.63–0.89	1.9	79.2	[32]	14	0.65–0.89	1.3	38.2
$C_{78}H_{158}$	[28]	15	0.63–0.88	0.63–0.88	1.7	79.6	[32]	14	0.65–0.88	0.9	39.3
$C_{79}H_{160}$	[28]	15	0.63–0.88	0.63–0.88	1.7	80.1	[32]	14	0.65–0.88	1.0	40.5
$C_{80}H_{162}$	[28]	15	0.63–0.88	0.63–0.88	1.7	80.5	[32]	14	0.65–0.88	0.9	41.6
$C_{81}H_{164}$	[28]	15	0.61–0.80	0.61–0.80	1.6	79.6	[32]	12	0.65–0.80	0.5	46.3
$C_{82}H_{166}$	[28]	14	0.62–0.80	0.62–0.80	2.0	80.0	[32]	12	0.65–0.80	0.4	47.4
$C_{83}H_{168}$	[28]	14	0.62–0.79	0.62–0.79	1.7	80.4	[32]	12	0.65–0.79	0.4	48.6
$C_{84}H_{170}$	[28]	14	0.65–0.88	0.65–0.88	2.2	82.1	[32]	14	0.65–0.88	1.3	46.0
$C_{85}H_{172}$	[28]	14	0.65–0.88	0.65–0.88	1.9	82.4	[32]	14	0.65–0.88	1.1	47.1
$C_{86}H_{174}$	[28]	14	0.65–0.88	0.65–0.88	1.9	82.8	[32]	14	0.65–0.88	1.2	48.2
$C_{87}H_{176}$	[28]	14	0.65–0.88	0.65–0.88	2.2	83.1	[32]	14	0.65–0.88	1.3	49.3
$C_{88}H_{178}$	[28]	14	0.65–0.88	0.65–0.88	2.0	83.4	[32]	14	0.65–0.88	1.4	50.4
$C_{89}H_{180}$	[28]	14	0.65–0.88	0.65–0.88	2.0	83.8	[32]	14	0.65–0.88	1.8	51.4
$C_{90}H_{182}$	[28]	14	0.64–0.88	0.64–0.88	2.3	84.1	[32]	14	0.64–0.88	1.6	52.5
$C_{91}H_{184}$	[28]	14	0.64–0.88	0.64–0.88	2.1	84.4	[32]	14	0.64–0.88	1.8	53.6
$C_{92}H_{186}$	[28]	14	0.64–0.88	0.64–0.88	2.2	84.7	[32]	14	0.64–0.88	2.2	54.6
$C_{93}H_{188}$	[28]	14	0.64–0.88	0.64–0.88	2.6	85.0	[32]	14	0.64–0.88	2.6	55.6
$C_{94}H_{190}$	[28]	14	0.64–0.88	0.64–0.88	2.3	85.3	[32]	14	0.64–0.88	2.3	56.7
$C_{95}H_{192}$	[28]	14	0.64–0.88	0.64–0.88	2.2	85.6	[32]	14	0.64–0.88	2.5	57.7
$C_{96}H_{194}$	[28]	14	0.64–0.88	0.64–0.88	2.2	85.8	[32]	14	0.64–0.88	2.9	58.7
$C_{97}H_{196}$	[28]	14	0.64–0.88	0.64–0.88	2.7	86.1	[32]	14	0.64–0.88	3.0	59.7
$C_{98}H_{198}$	[28]	14	0.64–0.88	0.64–0.88	2.3	86.4	[32]	13	0.66–0.88	3.3	59.0
$C_{99}H_{200}$	[28]	14	0.64–0.88	0.64–0.88	2.3	86.6	[32]	13	0.66–0.88	3.6	59.9
$C_{100}H_{202}$	[28]	14	0.64–0.88	0.64–0.88	2.8	86.9	[32]	13	0.66–0.88	4.2	60.9

Table A2
T_C, P_C, m, and ω optimized in this research and T_C, P_C, and ω from the correlations of Gao et al. [33] for n-alkanes from C_7 to C_{100}.

n-Alkanes	Optimized values in this research				Correlations of Gao et al. [33]		
	T_C/K	P_C/bar	m	ω	T_C/K	P_C/bar	ω
C_7H_{16}	542.48	27.73	0.8687	0.3407	540.40	27.497	0.3474
C_8H_{18}	570.59	25.74	0.9465	0.3986	569.44	25.142	0.3936
C_9H_{20}	595.96	23.97	1.0187	0.4536	595.30	23.097	0.4389
$C_{10}H_{22}$	618.54	22.35	1.0888	0.5043	618.53	21.304	0.4833
$C_{11}H_{24}$	628.90	21.03	1.1436	0.5456	639.55	19.717	0.5269
$C_{12}H_{26}$	657.99	19.81	1.2205	0.6042	658.69	18.302	0.5696
$C_{13}H_{28}$	666.68	18.65	1.2705	0.6426	676.19	17.034	0.6116
$C_{14}H_{30}$	694.01	17.65	1.3197	0.6808	692.28	15.891	0.6529
$C_{15}H_{32}$	698.81	17.01	1.3955	0.7401	707.12	14.856	0.6934
$C_{16}H_{34}$	723.05	16.06	1.4277	0.7657	720.86	13.915	0.7333
$C_{17}H_{36}$	729.58	15.23	1.4737	0.8024	733.61	13.057	0.7725
$C_{18}H_{38}$	751.46	14.86	1.5157	0.8358	745.48	12.271	0.8112
$C_{19}H_{40}$	764.37	14.31	1.5481	0.8618	756.56	11.549	0.8492
$C_{20}H_{42}$	777.28	13.66	1.5936	0.8988	766.91	10.884	0.8866
$C_{21}H_{44}$	787.93	13.09	1.6271	0.9261	776.61	10.271	0.9235
$C_{22}H_{46}$	796.83	12.67	1.6672	0.9589	785.71	9.704	0.9599
$C_{23}H_{48}$	810.48	12.30	1.6956	0.9824	794.27	9.178	0.9957
$C_{24}H_{50}$	821.85	11.95	1.7157	0.9990	802.33	8.690	1.0310
$C_{25}H_{52}$	830.97	11.58	1.7429	1.0216	809.92	8.235	1.0659
$C_{26}H_{54}$	841.21	11.26	1.7738	1.0474	817.09	7.812	1.1002
$C_{27}H_{56}$	849.96	10.96	1.7900	1.0609	823.87	7.417	1.1341
$C_{28}H_{58}$	859.36	10.70	1.8281	1.0930	830.28	7.048	1.1675
$C_{29}H_{60}$	867.48	10.41	1.8433	1.1058	836.35	6.702	1.2005
$C_{30}H_{62}$	876.02	10.27	1.8600	1.1200	842.11	6.378	1.2331
$C_{31}H_{64}$	883.77	9.98	1.8733	1.1313	847.58	6.074	1.2652
$C_{32}H_{66}$	891.11	9.81	1.8948	1.1496	852.77	5.788	1.2970
$C_{33}H_{68}$	899.07	9.67	1.9179	1.1693	857.71	5.519	1.3283
$C_{34}H_{70}$	905.91	9.43	1.9433	1.1911	862.41	5.266	1.3593
$C_{35}H_{72}$	911.58	9.29	1.9665	1.2110	866.88	5.028	1.3898
$C_{36}H_{74}$	918.25	9.16	1.9750	1.2184	871.14	4.803	1.4200
$C_{37}H_{76}$	924.99	8.98	2.0001	1.2400	875.21	4.591	1.4499
$C_{38}H_{78}$	930.93	8.81	2.0173	1.2549	879.08	4.390	1.4794
$C_{39}H_{80}$	936.66	8.64	2.0326	1.2683	882.79	4.200	1.5085
$C_{40}H_{82}$	940.00	8.43	2.0596	1.2918	886.32	4.021	1.5373
$C_{41}H_{84}$	946.66	8.28	2.0681	1.2993	889.71	3.851	1.5657
$C_{42}H_{86}$	951.88	8.16	2.0835	1.3127	892.94	3.690	1.5939
$C_{43}H_{88}$	955.98	8.02	2.1014	1.3285	896.03	3.537	1.6217
$C_{44}H_{90}$	961.81	7.88	2.1121	1.3379	899.00	3.391	1.6492
$C_{45}H_{92}$	965.59	7.69	2.1282	1.3521	901.84	3.254	1.6764

Table A2 (*Continued*)

n-Alkanes	Optimized values in this research				Correlations of Gao et al. [33]		
	T_C/K	P_C/bar	m	ω	T_C/K	P_C/bar	ω
$C_{46}H_{94}$	970.20	7.59	2.1433	1.3655	904.56	3.123	1.7033
$C_{47}H_{96}$	974.00	7.44	2.1602	1.3805	907.16	2.998	1.7299
$C_{48}H_{98}$	978.03	7.30	2.1714	1.3904	909.66	2.879	1.7562
$C_{49}H_{100}$	982.25	7.16	2.1832	1.4009	912.06	2.767	1.7822
$C_{50}H_{102}$	985.00	7.03	2.1947	1.4112	914.37	2.659	1.8080
$C_{51}H_{104}$	990.33	6.93	2.2088	1.4238	916.58	2.557	1.8334
$C_{52}H_{106}$	993.20	6.83	2.2092	1.4242	918.70	2.459	1.8586
$C_{53}H_{108}$	996.97	6.77	2.2185	1.4325	920.75	2.366	1.8836
$C_{54}H_{110}$	1000.64	6.69	2.2267	1.4398	922.71	2.277	1.9082
$C_{55}H_{112}$	1003.20	6.56	2.2404	1.4521	924.60	2.192	1.9327
$C_{56}H_{114}$	1006.68	6.48	2.2475	1.4585	926.42	2.111	1.9568
$C_{57}H_{116}$	1009.06	6.36	2.2610	1.4707	928.16	2.033	1.9808
$C_{58}H_{118}$	1012.36	6.28	2.2669	1.4760	929.85	1.959	2.0044
$C_{59}H_{120}$	1014.56	6.17	2.2800	1.4878	931.47	1.888	2.0279
$C_{60}H_{122}$	1017.69	6.10	2.2853	1.4926	933.03	1.820	2.0511
$C_{61}H_{124}$	1020.75	6.08	2.2938	1.5003	934.53	1.755	2.0741
$C_{62}H_{126}$	1022.71	5.94	2.3037	1.5093	935.98	1.693	2.0968
$C_{63}H_{128}$	1025.62	5.91	2.3112	1.5161	937.38	1.633	2.1193
$C_{64}H_{130}$	1027.42	5.79	2.3216	1.5255	938.73	1.576	2.1416
$C_{65}H_{132}$	1030.20	5.75	2.3275	1.5309	940.02	1.521	2.1637
$C_{66}H_{134}$	1032.91	5.65	2.3271	1.5305	941.28	1.469	2.1856
$C_{67}H_{136}$	1034.52	5.60	2.3429	1.5449	942.49	1.419	2.2072
$C_{68}H_{138}$	1038.14	5.52	2.3333	1.5362	943.66	1.370	2.2287
$C_{69}H_{140}$	1038.59	5.46	2.3577	1.5584	944.78	1.324	2.2499
$C_{70}H_{142}$	1042.09	5.39	2.3486	1.5501	945.87	1.279	2.2710
$C_{71}H_{144}$	1043.48	5.33	2.3622	1.5625	946.92	1.236	2.2918
$C_{72}H_{146}$	1045.83	5.26	2.3625	1.5628	947.94	1.195	2.3125
$C_{73}H_{148}$	1047.11	5.21	2.3753	1.5745	948.92	1.156	2.3330
$C_{74}H_{150}$	1050.40	5.15	2.3652	1.5653	949.87	1.118	2.3532
$C_{75}H_{152}$	1050.53	5.10	2.3882	1.5864	950.79	1.081	2.3733
$C_{76}H_{154}$	1053.73	5.03	2.3756	1.5748	951.67	1.046	2.3932
$C_{77}H_{156}$	1053.77	5.00	2.4006	1.5978	952.53	1.012	2.4129
$C_{78}H_{158}$	1056.87	4.94	2.3887	1.5868	953.36	0.980	2.4325
$C_{79}H_{160}$	1058.92	4.88	2.3925	1.5903	954.16	0.948	2.4518
$C_{80}H_{162}$	1059.86	4.83	2.3983	1.5957	954.94	0.918	2.4710
$C_{81}H_{164}$	1061.80	4.78	2.3977	1.5951	955.69	0.889	2.4901
$C_{82}H_{166}$	1061.61	4.73	2.4196	1.6153	956.42	0.861	2.5089
$C_{83}H_{168}$	1064.53	4.68	2.4069	1.6036	957.12	0.834	2.5276
$C_{84}H_{170}$	1065.31	4.66	2.4206	1.6162	957.81	0.808	2.5461
$C_{85}H_{172}$	1067.11	4.59	2.4165	1.6124	958.47	0.783	2.5645
$C_{86}H_{174}$	1067.80	4.54	2.4247	1.6200	959.11	0.759	2.5826
$C_{87}H_{176}$	1069.54	4.52	2.4259	1.6211	959.73	0.736	2.6007
$C_{88}H_{178}$	1070.17	4.46	2.4334	1.6280	960.33	0.713	2.6185
$C_{89}H_{180}$	1070.78	4.41	2.4455	1.6392	960.91	0.692	2.6363
$C_{90}H_{182}$	1072.40	4.39	2.4405	1.6346	961.47	0.671	2.6538
$C_{91}H_{184}$	1072.92	4.33	2.4470	1.6406	962.02	0.651	2.6713
$C_{92}H_{186}$	1073.45	4.29	2.4596	1.6523	962.55	0.631	2.6885
$C_{93}H_{188}$	1073.90	4.27	2.4645	1.6568	963.06	0.612	2.7056
$C_{94}H_{190}$	1075.44	4.22	2.4596	1.6523	963.56	0.594	2.7226
$C_{95}H_{192}$	1075.84	4.17	2.4664	1.6586	964.05	0.577	2.7395
$C_{96}H_{194}$	1076.21	4.13	2.4773	1.6687	964.52	0.560	2.7561
$C_{97}H_{196}$	1077.66	4.12	2.4716	1.6634	964.97	0.543	2.7727
$C_{98}H_{198}$	1077.99	4.06	2.4775	1.6689	965.41	0.527	2.7891
$C_{99}H_{200}$	1078.28	4.02	2.4842	1.6751	965.84	0.512	2.8054
$C_{100}H_{202}$	1078.55	4.01	2.4940	1.6842	966.26	0.497	2.8215

research require less perturbation from P_{CP} to obtain more accurate density predictions for oils lighter than 25°API. For such lighter oils, it is likely that the concentration of paraffinic components is relatively high.

Fig. 21 also show that AADs in density predictions for five oils heavier than 25°API (22.6, 13.38, 11.98, 11.63, and 9.5°API) are larger when Eqs. (11)–(13) are used. Using these equations, however, smaller perturbations of P_C are required to match measured saturation pressures even for these five heavy oils as given in Table 4. Reliable characterization for these low-API reservoir oils using the PR EOS were recently developed based on a new perturbation method with the critical parameters developed in this research (Kumar and Okuno [18]).

5. Conclusions

We developed correlations for critical temperatures (T_C), critical pressures (P_C), and acentric factors (ω) that are optimized for phase behavior modeling of n-alkanes from C_7 to C_{100} using the Peng–Robinson (PR) EOS. The optimization used 3583 density data and 1525 vapor pressure data available in the literature. The new set of T_C, P_C, and ω satisfies Pitzer's definition of ω. The optimum T_C, P_C, and ω values were applied to predict phase behavior of n-alkane mixtures and 25 different reservoir oils using the PR EOS. The conclusions are as follows:

1. The PR EOS with the optimized T_C, P_C, and ω (Table A2) results in 2.8% AAD in density prediction and 1.6% in vapor pressure prediction for n-alkanes from C_7 to C_{100}.

2. The PR EOS with our correlations for T_C, P_C, and ω (Eqs. (11)–(13)) gives 3.0% and 3.4% AADs in density and vapor pressure predictions, respectively, for n-alkanes from C_7 to C_{100}. When conventional correlations are used for critical parameters, the PR EOS exhibits less accurate predictions for heavier n-alkanes, and AADs can be as high as 61% for vapor pressure prediction and 87% for density prediction for n-C_{100}.
3. The critical parameter correlations developed in this research significantly improve phase behavior predictions for n-alkane mixtures. Use of conventional correlations for critical parameters available in the literature results in larger AADs in density prediction and bubble- and dew-point predictions. The errors are more significant for heavier n-alkane mixtures using the conventional correlations.
4. The critical parameters for n-alkanes developed provide useful initial values for characterization of reservoir oils using the PR EOS. Results showed that, when perturbation of P_C from the n-alkane values is used to match experimental data, resulting values for P_C are greater than the n-alkane values. This is because aromatic and naphthenic components have higher critical pressures than n-alkanes for a given carbon number group. The new set of T_C and P_C correlations for a homologous series of n-alkanes can serve as the lower bounds for T_C and P_C of pseudo components of reservoir fluids characterized using the PR EOS.
5. The PR EOS with the critical parameters developed in this research exhibits improved predictive capability for oils lighter than 25°API, where concentrations of aromatic and naphthenic components are typically insignificant.

List of symbols

b	covolume parameter in a cubic EOS
f	perturbation factor defined in Section 4.2
m	$m(\omega)$ function in the PR EOS given in Eqs. (4) and (5)
P	pressure, bar
P_C	critical pressure, bar
P_{CP}	critical pressure for a paraffinic component, bar
P_r	reduced pressure
P_r^{vap}	reduced vapor pressure
P_{SAT}	saturation pressure, bar
T	temperature, K
T_C	critical temperature, K
T_r	reduced temperature
v	molar volume

Greek letters

$\alpha(T)$	alpha function in the PR EOS
ω	acentric factor

Abbreviations

AAD	average absolute deviation
CN	carbon number
EOS	equation of state
MW	molecular weight
NBP	normal boiling point K
PNA	paraffins, naphthenes, and aromatics
PR	Peng–Robinson
SRK	Soave–Redlich–Kwong

Appendix A.

Tables A1 and A2

References

[1] J.D. van der Waals, Over de Continuiteit van den Gas-en Vloeistoftoestand, Ph.D. dissertation (excerpt), Leiden, The Netherlands, 1873.
[2] D.Y. Peng, D.B. Robinson, Ind. Eng. Chem. Fundam. 15 (1976) 59–64.
[3] D.B. Robinson, D.Y. Peng, Gas Processors Association Research Report RR-28, 1978.
[4] G. Soave, Chem. Eng. Sci. 27 (1972) 1197–1203.
[5] R. Okuno, R.T. Johns, K. Sepehrnoori, SPE J. 16 (2011) 751–767.
[6] K.S. Pedersen, A.L. Blilie, K.K. Meisingset, Ind. Eng. Chem. Res. 31 (1992) 1378–1384.
[7] E. Neau, J.N. Jaubert, Ind. Eng. Chem. Res. 32 (1993) 1196–1203.
[8] PVTsim, 20.0, CALSEP International Consultants, Copenhagen, Denmark, 2011.
[9] M.R. Riazi, Manual 50, Characterization and Properties of Petroleum Fractions, ASTM International, West Conshohocken, PA, 2005.
[10] K.S. Pedersen, P.L. Christensen, Phase Behavior of Petroleum Reservoir Fluid, Taylor & Francis, Boca Raton, FL, USA, 2007.
[11] C.H. Whitson, M.R. Brulé, Phase Behavior SPE Monograph Volume 20, Society of Petroleum Engineers, Richardson, TX, USA, 2000.
[12] D. Ambrose, C. Tsonopoulos, J. Chem. Eng. Data 40 (1995) 531–546.
[13] S.M. Klara, K. Hemanth-Kumar, Society of Petroleum Engineers, SPE-16942, in: Presented at SPE Annual Technical Conference and Exhibition, Dallas, TX, 27–30 September, 1987.
[14] M. Voulgaris, S. Stamatakis, D. Tassios, Fluid Phase Equilib. 64 (1991) 73–106.
[15] I. Rodríguez, A.A. Hamouda, Society of Petroleum Engineers, SPE-117446, in: Presented at SPE International Thermal Operations and Heavy Oil Symposium, Calgary, Canada, 20–23 October, 2008.
[16] A. Péneloux, E. Rauzy, R. Fréze, Fluid Phase Equilib. 8 (1982) 7–23.
[17] B.S. Jhaveri, G.K. Youngren, SPE J. 3 (1988) 1033–1040.
[18] A. Kumar, R. Okuno, SPE J., submitted for publication on June 18, 2012.
[19] P.M. Mathias, Ind. Eng. Chem. Process. Des. Dev. 22 (1983) 385–391.
[20] R. Stryjek, J.H. Vera, Can. J. Chem. Eng. 64 (1986) 323–333.
[21] G.A. Melhem, R. Saini, B.M. Goodwin, Fluid Phase Equilib. 47 (1989) 189–237.
[22] H. Li, D. Yang, Energ. Fuel. 25 (2011) 215–223.
[23] G.N. Nji, W.Y. Svrcek, H. Yarranton, M.A. Satyro, Energ. Fuel. 22 (2008) 455–462.
[24] G.N. Nji, W.Y. Svrcek, H. Yarranton, M.A. Satyro, Energ. Fuel. 23 (2009) 366–373.
[25] P.D. Ting, P.C. Joyce, P.K. Jog, W.G. Chapman, M.C. Thies, Fluid Phase Equilib. 206 (2003) 267–286.
[26] E.C. Voutsas, G.D. Pappa, K. Magoulas, D.P. Tassios, Fluid Phase Equilib. 240 (2006) 127–139.
[27] S.E. Quiñones-Cisneros, C.K. Zéberg-Mikkelsen, E.H. Stenby, Fluid Phase Equilib. 212 (2003) 233–243.
[28] C.L. Yaws, Yaws' Thermo Physical Properties of Chemicals and Hydrocarbons (Electronic Edition), Knovel, New York, USA, 2010.
[29] H.G. Rackett, J. Chem. Eng. Data 15 (1970) 514–517.
[30] T.E. Daubert, R.P. Danner, H.M. Sibel, C.C. Stebbins, Physical and Thermodynamic Properties of Pure Chemicals: Data Compilation, Taylor & Francis, Washington, DC, 1997.
[31] B.E. Poling, J.M. Prausnitz, J.P. O'Connell, The Properties of Gases and Liquids, The McGraw-Hill, New York, NY, 2001.
[32] M.R. Riazi, Y.S. AlQaheem, Ind. Eng. Chem. Res. 49 (2010) 7104–7112.
[33] W. Gao, R.L. Robinson Jr., K.A.M. Gasem, Fluid Phase Equilib. 179 (2001) 207–216.
[34] DECHEMA Gesellschaft für Chemische Technik und Biotechnologie, http://i-systems.dechema.de/detherm/mixture.php.
[35] M.R. Riazi, T.A. Al-Sahhaf, Fluid Phase Equilib. 117 (1996) 217–224.
[36] A. Aucejo, M.C. Burguet, R. Muñoz, J.L. Marques, J. Chem. Eng. Data 40 (1995) 141–147.
[37] A.J. Queimada, I.M. Marrucho, J.A.P. Coutinho, E.H. Stenby, Int. J. Thermophys. 26 (2005) 47–61.
[38] C.J. Peter, J. de Swan Arons, J.M.H. Levelt Sengers, J.S. Gallagher, AIChE J. 34 (1988) 834–839.
[39] C.J. Peter, J. Spiegelaar, J. de Swan Arons, Fluid Phase Equilib. 41 (1988) 245–256.
[40] P.C. Joyce, M.C. Thies, J. Chem. Eng. Data 43 (1998) 819–822.
[41] P.C. Joyce, J. Gordon, M.C. Thies, J. Chem. Eng. Data 45 (2000) 424–427.
[42] S.E. Quiñones-Cisneros, S.I. Andersen, J. Creek, Energ. Fuel. 19 (2005) 1314–1318.
[43] S.E. Quiñones-Cisneros, C.K. Zéberg-Mikkelsen, A. Baylaucq, C. Boned, Int. J. Thermophys. 25 (2004) 1353–1366.
[44] S.E. Quiñones-Cisneros, A. Dalberg, E.H. Stenby, Pet. Sci. Technol. 22 (2004) 1309–1325.
[45] K.H. Coats, G.T. Smart, SPE Reserv. Eng. 1 (1986) 277–299.
[46] A.S. Cullick, F.N. Pebdani, A.K. Griewank, Ind. Eng. Chem. Res. 28 (1989) 340–347.
[47] K. Krejbjerg, K.S. Pedersen, Canadian International Petroleum Conference, 57th Annual Technical Meeting, Calgary, Canada, June 13–15, 2006.
[48] S. Patil, A. Dandekar, S. Khataniar, Project Report, DOE Award No. DE-FC26-01NT41248, 2008, http://www.osti.gov/bridge/purl.cover.jsp?purl=/963365-YrCq8p/963365.pdf.
[49] A.K. Doolittle, J. Chem. Eng. Data 9 (1964) 275–279.
[50] G. Schilling, R. Kleinrahm, W. Wagner, J. Chem. Thermodyn. 40 (2008) 1095–1105.
[51] A.R. Goodwin, C.H. Bradsell, L.S. Toczylkin, J. Chem. Thermodyn. 28 (1996) 637–646.
[52] R.H. Perry, D.W. Green, Perry's Chemical Engineers' Handbook, 8th edition, The McGraw Hill Companies, Inc., New York, USA, 2007.

[53] S.S. Susnar, C.J. Budziak, H.A. Hamza, A.W. Neuman, Int. J. Thermophys. 13 (1992) 443–452.
[54] T.S. Banipal, S.K. Garg, J.C. Ahluwalia, J. Chem. Thermodyn. 23 (1991) 923–931.
[55] O. Elizalde-Solis, L.A. Galicia-Luna, L.E. Camacho-Camacho, Fluid Phase Equilib. 259 (2007) 23–32.
[56] T.S. Khasanshin, A.P. Shchemelev, High Temp. 40 (2002) 235–239.
[57] J.L. Daridon, H. Carrier, B. Lagourette, Int. J. Thermophys. 23 (2002) 697–708.
[58] S. Dutour, J.L. Daridon, B. Lagourette, Int. J. Thermophys. 21 (2000) 73–184.
[59] S. Dutour, B. Lagourette, J.L. Daridon, J. Chem. Thermodyn. 33 (2001) 765–774.
[60] S. Dutour, B. Lagourette, J.L. Daridon, J. Chem. Thermodyn. 34 (2002) 475–484.
[61] M.B. Ewing, J.C.S. Ochoa, J. Chem. Eng. Data 50 (2005) 1543–1547.
[62] J. Gregorowicz, K. Kiciak, S. Malanowski, Fluid Phase Equilib. 38 (1987) 97–107.
[63] D.L. Morgan, R. Kobayashi, Fluid Phase Equilib. 97 (1994) 211–242.